Positronium Cooling and Emission in Vacuum from Nanochannels at Cryogenic Temperature

Sebastiano Mariazzi,[1] Paolo Bettotti,[2] and Roberto S. Brusa[1]

[1]*Dipartimento di Fisica, Università di Trento and INFN, Gruppo collegato di Trento, Via Sommarive 14, I-38050 Povo, Trento, Italy*
[2]*Laboratorio di Nanoscienze, Dipartimento di Fisica, Università di Trento, Via Sommarive 14, I-38050 Povo, Trento, Italy*
(Received 20 January 2010; published 16 June 2010)

High formation yield and a meaningful cooled fraction of positronium below room temperature were obtained by implanting positrons in a silicon target in which well-controlled oxidized nanochannels (5–8 nm in diameter) perpendicular to the surface were produced. We show that by implanting positrons at 7 keV in the target held at 150 K, about 27% of positrons form positronium that escapes into the vacuum. Around 9% of the escaped positronium is cooled by collision with the walls of nanochannels and is emitted with a Maxwellian beam at 150 K. Because positronium quantum confinement limits the minimum achievable positronium energy, the tuning of the nanochannel's size is crucial for obtaining positronium gases in vacuum at very low temperature.

Advanced experiments such as positronium Bose-Einstein condensation [1], gravitational and spectroscopy studies with antihydrogen obtained by charge-exchange process between positronium atoms and antiprotons [2,3], high precision spectroscopy, and excitation measurements [4] of positronium, may be feasible provided that a dense gas of cooled positronium atoms at cryogenic temperature is produced and confined into nanosize cavities or free in vacuum.

Positronium (Ps), the bound state of an electron and a positron, can be formed by implanting positrons with energies of few keV in solids [5,6]. Injected positrons slow down reaching their thermal energy in few picoseconds; then they start a diffusive motion. Positrons are prevented from forming Ps into the bulk of metals and semiconductors because of the high electronic density, but it can be formed by positrons diffusing back to the surface where the electronic density is lower [6]. In insulators, Ps formation at the surface is usually forbidden for thermalized positrons because of the high electron ionization energy necessary to extract an electron. Previous studies showed that a small fraction of Ps was formed by epithermal positrons [7] and by a thermal activated emission in which positrons trapped at the surface were detrapped as Ps [8]. Differently, in many insulators, Ps formation is known to occur in the bulk. Ps which reaches the surface of an insulator can be emitted into the vacuum provided that its work function is negative [6]. Ps can also be emitted and trapped in subnanosize or nanosize open volume defects in insulators. Indeed when a network of connected open volume defects is present, Ps can be emitted into the vacuum after a hopping diffusion [9].

Recent developments in positron traps [10] have allowed experiments with many positrons in porous silica. The formation of Ps_2 molecule was inferred [11,12] and the cross section of Ps-Ps spin exchange quenching was evaluated [12]. Future challenging experiments require the cooling of Ps [1–4]. An intense research activity is underway to find materials that are suitable Ps converters and that present the right morphology for an efficient cooling of Ps.

Thermal Ps at temperatures lower than 150 K was found to be emitted by an Al surface on which few oxygen layers were grown [13]. Nevertheless this system requires highly controlled growing conditions and the oxygen overlayer was found to be very sensitive to changes in sample temperature and to photon flux exposure, which prevents the use of Al as a converter at low temperature [14].

In porous silica materials Ps is efficiently formed (more than 50% of implanted positrons) [15] and it is emitted inside the pores with a kinetic energy spectrum centered around 1–3 eV [16]. Ps loses its energy and cools down through collisions with the walls of the pores. Cooling below room temperature (RT) by this process was shown only in compressed silica powder [17]. Because of its short lifetime of 125 ps in vacuum, the singlet state of Ps [i.e., parapositronium (p-Ps) annihilating in 2γ] is completely lost in the cooling process. Conversely, the longer lifetime in vacuum of 142 ns of the triplet state [i.e., orthopositronium (o-Ps) annihilating into 3γ] allows it to reach the vacuum with lower kinetic energy. In each collision, the positron of the Ps atom has a probability of annihilation in 2γ with an electron of opposite spin of the medium (pick-off annihilation). The unavoidable pickoff annihilations reduce the Ps cooled fraction. Several porous silica-based materials with disordered porosities were investigated and a fraction of Ps was found to escape from the samples with mean energy slightly higher than thermal [18–23]. No measurements on these materials at cryogenic temperature were reported.

In this work we have followed a completely different strategy for producing and cooling Ps. The behavior of a new material with regular nanostructures instead of silica disordered systems has been investigated. The rationale is that the regular nanostructures may allow a better control of cooled Ps beams in vacuum and of Ps confinement [24]. The minimum energy that Ps can reach is set by the size of

the nanopores in which it is emitted while the emission angle from open porosities is expected to depend upon the size of the channel and its temperature [24].

In this experiment, nanochannels perpendicular to the surface were realized by an electrochemical etching of Si in a HF solution. To obtain Ps formation and emission into the vacuum, the inner surface of the nanochannels was oxidized. The presented yield and velocity measurements of Ps have been done on a target for which the synthesis parameters were optimized to obtain nanochannels with a diameter between 5–8 nm and a length of $\sim$2.0 μm. Specifically, we set 10 mA/cm^2 etching current and 15-min etching time, and 30% HF concentration and 2 h oxidation time in air. A Si p-type (100) with resistivity 0.15–0.21 Ω cm was chosen as basic material. The size of the nanochannels was checked by high resolution scanning electron microscopy. The nanochannels were found to be spaced by about their size and the etched layer was estimated to have a density $\rho = 1.9$ g/cm^3. Ps yield and time of flight (TOF) measurements of Ps velocity were carried out with an energy tunable slow positron beam. The positron spot on the sample was about 1 mm.

The calibrated fraction $F_{3\gamma}(E)$ of implanted positrons at energy E forming o-Ps annihilating by 3γ is shown in Fig. 1 for RT, 200, and 150 K. The $F_{3\gamma}(E)$ was calculated as the ratio of the 2γ annihilations in the 511 keV annihilation peak and the 3γ annihilations in the area below the peak [25] after calibration with a Ge crystal held at 1000 K to have 0% and 100% Ps formation in the present experimental conditions [25,26]. The error on $F_{3\gamma}(E)$, both due to 0% and 100% evaluation, was less than 3.5% [26]. The
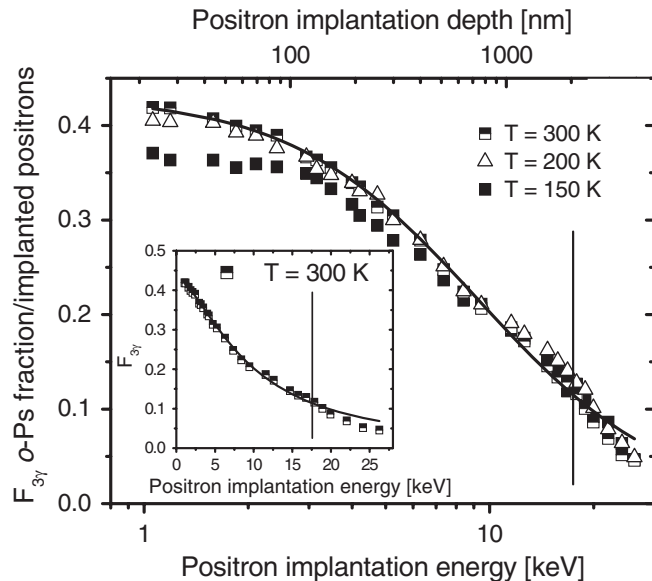
temperature of 150 K is the lowest one permitted in our set up for measuring Ps velocity. Because of the low intensity of the positron beam ($2 \times 10^4 e^+$/s), the measurements took 14 days for spectrum. The build up of contaminants (in particular H_2O) on the sample was minimized by working at a vacuum condition of 1×10^{-9} mbar at 150 K. The continuous lines through the experimental $F_{3\gamma}(E)$ points are a best fit with a model based on the Ps diffusion equation [9,27]. The fitting procedure gave an estimation of the fraction of o-Ps escaping outside the target into the vacuum, the o-Ps formation, and o-Ps annihilating by 3γ inside the nanochannels. Almost the total amount of observed o-Ps in Fig. 1 was found to escape into the vacuum. The fraction of o-Ps annihilating via 3γ inside the nanochannels was less than 0.5% of the implanted positrons and the extracted o-Ps diffusion length was $L_{Ps} = 743 \pm 15$ nm, which is consistent with the high o-Ps emission and the channel length of about 2 μm. At 1 keV positron implantation energy, the escaping o-Ps was more than 40% of the implanted positrons, increasing the implantation energy this fraction decreased due to pickoff. At a positron implantation energy of 9.3 keV, corresponding to $L_{Ps} = 743$ nm, half (20%) of Ps atoms escape from the channels. At each positron implantation energy the lost o-Ps fraction could be read as the difference between the observed o-Ps value $F_{3\gamma}(E)$ and the maximum value of the curve. We note that the data of Fig. 1 are well described assuming a constant diffusion coefficient, whose value can be estimated as $D_{Ps} = L_{Ps}^2/\tau \cong 0.069 \pm 0.003$ cm^2 s^{-1} using the calculated mean Ps lifetime $\tau \cong 80$ ns in a cavity of about 5–8 nm in diameter [28].

The high yield of Ps is due to the novel design of the present target that utilizes both the properties of bulk Si and of the silicon oxide. The cascade of physical processes that leads to Ps emission are likely the following: (a) thermalized positrons in bulk Si have diffusion length of $\sim$200 nm [5]; (b) due to the high diffusion length and to the closeness of nanochannels, the majority of positrons reach the Si-silicon oxide interface; (c) there, positrons are energetically allowed to reach the silicon oxide [29]; (d) wherein positrons can efficiently form Ps [30]; and (e) after a very short diffusion path, formed Ps atoms reach the inner surface of the nanochannels and are emitted. A fraction of Ps, formed by epithermal positrons, is also expected.

The o-Ps velocity perpendicular to the target surface was measured by a TOF apparatus detecting the time between positron implantation in the target and o-Ps annihilation in flight. The signal of positron arrival was derived by detecting the emitted secondary electrons with a channeltron. The gamma rays emitted by o-Ps self annihilation were detected with a NaI (Tl) scintillator placed behind an 11 cm thick tungsten shield, with a slit of 5 mm width. The center of the slit was located at $z_0 = 8.9$ mm from the target surface which represents the flight path of o-Ps during its lifetime. More than 2×10^3 events were collected for each

FIG. 1. o-Ps fraction vs positron implantation energy (lower scale) and mean positron implantation depth $\bar{z}$ (upper scale). The continuous lines are best fits to the data. The vertical lines mark the border between the Si layer with channels and the Si bulk. The RT curve in a linear scale is shown in the inset. The error bars are inside the symbols.

TOF spectrum using a time-to-amplitude converter and a multichannel analyzer. The FWHM of the prompt peak, due to 511 keV positron annihilations, was 23 ns [inset in Fig. 2]. The as-recorded TOF spectra were smoothed through a moving average filtering on 61 channels (0.137 ns/channel). The background originating from gammas due to prompt positron annihilation and scattered into the slit was subtracted and the effects of o-Ps finite lifetime and permanence in front to the slit were corrected by multiplying by $\frac{1}{t}e^{t/(142 \text{ ns})}$ [31]. The measured time of flight t was converted to the o-Ps kinetic energy $E_\perp$ by the relationship $E_\perp = m_0(z_0/t)^2$, where m_0 is the positron rest mass. The TOF spectra have an asymmetric shape with a peak at higher emission energies [Fig. 2] due to o-Ps exiting the channel after few collisions. This shape is a consequence of the regular channel structure, perpendicular to the surface of the target. Increasing the positron implantation energy from 4 to 7 keV, the escaping o-Ps fraction [Fig. 1] and the average o-Ps emission energy

[Fig. 2] decrease from 30% to 25% and from 140 to 96 meV, respectively. The decrease of average emission energy is related to the increase of collisions when Ps is formed deeper in the target. At 7 keV, a decrease of the target temperature from RT to 200 and further to 150 K leads to an almost linear decrease of the average o-Ps emission energy to 76 meV and to 68 meV, respectively, [Fig. 2]. The thermalized o-Ps fraction could be evaluated from the tail area of the spectra, i.e., from $t_M = z_0/v_{\text{th}}$ to the end of the distribution [where $v_{\text{th}} = \sqrt{3k_BT/(2m_0)}$ is the o-Ps velocity corresponding to the sample temperature T, and k_B is the Boltzman constant]. At RT, 200, and 150 K, a thermalized o-Ps fraction of $\sim$19%, $\sim$15%, and $\sim$9% is emitted, respectively. Since about 27% of o-Ps escapes into the vacuum at 7 keV positron implantation energy [Fig. 1)], it can be estimated that about 5%, 4%, and 2.5% of the implanted positrons produce thermal o-Ps in vacuum at RT, 200, and 150 K, respectively.

In principle, the time of Ps emission from the sample is not known in the TOF measurements and should be subtracted from the measured time of flight. For Ps formed at high depth we can estimate, in the frame of the diffusion model, a mean time $\bar{t} = \bar{z}^2/(2D_{\text{Ps}})$ of permanence in the channel before emission, as a function of the depth $\bar{z} = (\frac{40}{1.9 \text{ g/cm}^3})(E \text{ keV})^{1.6}$ [5,23]. From a depth corresponding to 7 keV and with the above calculated D_{Ps}, Ps escapes with a mean escaping time $\bar{t} \cong 16 \pm 1$ ns in the present samples. This short permanence time of Ps in the channels does not affect significantly our TOF spectra. Different conditions could arise in disordered porous materials with porosities of 2–3 nm in size where the diffusion of Ps was found to be 2 times lower [23] than in the present case.

To find the maximum yield of thermal Ps, a fine-tuning of positron implantation energy would be necessary. Lowering the temperature of the samples, the thermalization time increases [24], and probably the positron implantation energy would be tuned at higher energy with respect to RT to obtain the same yield of thermalized Ps.

The observed slight decrease in the intensity of Ps yield with decreasing the temperature in Fig. 2, and not observed in Fig. 1, is not yet completely understood but could be related both to some kind of aging of the inner surface of the nanochannels or to a not perfect tuning of the positron implantation energy for obtaining the maximum Ps yield at this temperature.

The o-Ps energy spectra obtained by multiplying the TOF spectra of Fig. 2 by t^3 are shown in Fig. 3 in a semilog scale. The energy spectra below 0.25 eV are well fitted by two exponentials corresponding to two well-defined Maxwellian beams at the temperature reported in the figure. The low energy part is due to the distribution of positrons cooled at the sample temperature. The two well-distinct distributions could be explained by the fact that in about straight and regular nanochannels where Ps has a high diffusivity, only Ps formed around a precise depth corresponding to the short mean escaping time has
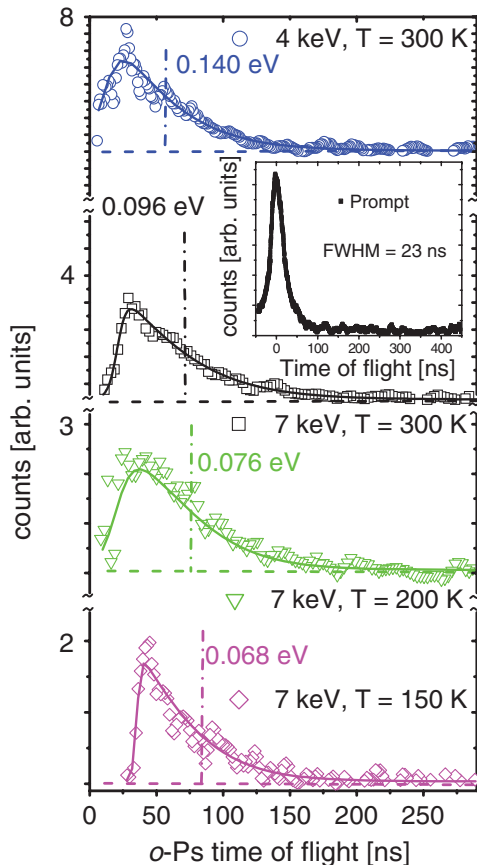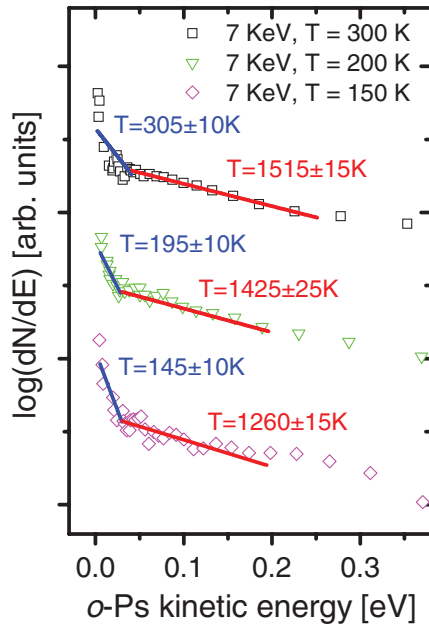
FIG. 2 (color). Room temperature o-Ps TOF spectra at 4 and 7 keV positron implantation energy and spectra at 7 keV lowering the target temperature to 200 and 150 K. The average time t_a of the o-Ps TOF distribution is marked by vertical dash-dotted lines. The o-Ps energy, $E_\perp$, corresponding to t_a is reported. The continuous lines are fits with an asymmetrical double sigmoidal function to guide the eye. In the inset, the positron annihilation prompt peak is reported. Zero counts are indicated by horizontal dashed lines.

FIG. 3 (color).   o-Ps energy spectra in a semilog scale obtained by multiplying by t^3 the data of Fig. 2. The two-exponential fits for each spectrum point out the presence of two different Maxwellian beam distributions at the indicated temperature.

the chance to thermalize and to be emitted into the vacuum. In the present case the escaping time was found to be about 2 times the thermalization time [24]. At the contrary, in disordered porous materials with optimized porous size for thermalization, thermalized Ps is expected to escape from different depths at a given positron implantation energy because of the tortuosity of the diffusion paths.

With the actually available apparatuses [10–12] producing positron bunches of 2×10^8–$10^9 e^+$, about 5×10^6–10^7 o-Ps thermalized atoms at 150 K could be obtained with the present target. Thus this o-Ps cooled beam can meet the requirement for spectroscopic experiment and production of antihydrogen beams.

The possibility of tuning the dimension of channels is crucial for Ps cooling. Indeed, the minimum temperature that o-Ps can achieve by collision in nanochannels depends on their dimension because of o-Ps quantum confinement [24]. If the nanochannel is approximated by an infinitive potential well with a quadratic base of side a, the minimum temperature of o-Ps in its ground state is $T = \frac{\hbar^2 \pi^2}{3 k_B m_0 a^2}$, where $\hbar$ is the reduced Planck constant. This relation points out that the size of nanochannels must be >5 nm to cool o-Ps below 115 K. To reach 7 K the size should be increased to 20 nm. A drawback is that an increase in size results in longer thermalization times [24,32], so that for each experiment the right balance should be found.

The quantum confinement can also influence the angular distribution of the thermalized emitted Ps atoms [24]. If Ps is quantum confined into a channel, it totally loses its velocity in the channel direction when its energy is close

to the ground state. Thus, a fraction of Ps could escape with a wider angle with respect to the normal to the sample. In a TOF experiment, this will result in a reduction of detected events in the thermal region of the spectra. Here, with channel size >5 nm and a sample temperature of 150 K, we are intentionally far from this condition and the angular distribution is not expected to vary going from RT to 150 K.

[1] P. M. Platzman and A. P. Mills, Jr., Phys. Rev. B **49**, 454 (1994).
[2] P. Perez and A. Rosowsky, Nucl. Instrum. Methods Phys. Res., Sect. A **545**, 20 (2005).
[3] A. Kellerbauer et al., Nucl. Instrum. Methods Phys. Res., Sect. B **266**, 351 (2008).
[4] F. Castelli et al., Phys. Rev. A **78**, 052512 (2008).
[5] P. J. Schultz, and K. G. Lynn, Rev. Mod. Phys. **60**, 701 (1988).
[6] A. P. Mills, Jr., in Positron Spectroscopy of Solids, edited by A. Dupasquier and A. P. Mills, Jr. (IOS Press, Amsterdam, 1995), p. 209.
[7] P. Sferlazzo, S. Berko, and K. F. Canter, Phys. Rev. B **35**, 5315 (1987).
[8] P. Sferlazzo, S. Berko, and K. F. Canter, Phys. Rev. B **32**, 6067 (1985).
[9] M. P. Petkov et al., Appl. Phys. Lett. **79**, 3884 (2001).
[10] C. M. Surko and R. G. Greaves, Phys. Plasmas **11**, 2333 (2004).
[11] D. B. Cassidy and A. P. Mills, Jr., Nature (London) **449**, 195 (2007).
[12] D. B. Cassidy and A. P. Mills, Jr., Phys. Rev. Lett. **100**, 013401 (2008).
[13] A. P. Mills, Jr. et al., Phys. Rev. B **44**, 5791 (1991).
[14] M. S. Fee et al., Phys. Rev. A **48**, 192 (1993).
[15] M. P. Petkov et al., J. Phys. Chem. B **107**, 2725 (2003).
[16] Y. Nagashima et al., Phys. Rev. B **58**, 12676 (1998).
[17] A. P. Mills, Jr. et al., Phys. Rev. B **40**, 2045 (1989).
[18] R. S. Vallery, P. W. Zitzewitz, and D. W. Gidley, Phys. Rev. Lett. **90**, 203402 (2003).
[19] K. Ito et al., J. Appl. Phys. **98**, 094307 (2005).
[20] C. He et al., Phys. Rev. B **75**, 195404 (2007).
[21] L. Liszkay et al., Appl. Surf. Sci. **255**, 187 (2008).
[22] H. K. M. Tanaka, T. Kurihara, and A. P. Mills, Jr., J. Phys. Condens. Matter **18**, 8581 (2006).
[23] D. B. Cassidy et al., Phys. Rev. A **81**, 012715 (2010).
[24] S. Mariazzi, A. Salemi, and R. S. Brusa, Phys. Rev. B **78**, 085428 (2008).
[25] R. S. Brusa et al., Acta Phys. Pol. A **107**, 702 (2005).
[26] E. Soininen, A. Schwab, and K. G. Lynn, Phys. Rev. B **43**, 10051 (1991).
[27] M. Eldrup et al., Phys. Rev. B **32**, 7048 (1985).
[28] T. L. Dull et al., J. Phys. Chem. B **105**, 4657 (2001).
[29] G. Brauer et al., Phys. Rev. B **66**, 195331 (2002).
[30] S. Van Petegem et al., Phys. Rev. B **70**, 115410 (2004).
[31] R. H. Howell et al., Phys. Rev. B **35**, 5303 (1987).
[32] Y. Nagashima et al., Phys. Rev. A **52**, 258 (1995).